https://doi.org/10.5194/acp-2020-110
Preprint. Discussion started: 27 February 2020

Atmospheric Chemistry and Physics Discussions

An investigation on hygroscopic properties of 15 black carbon (BC) from different carbon sources: Roles of organic and inorganic components

Minli Wang[a], Yiqun Chen[a], Heyun Fu[a], Xiaolei Qu[a], Bengang Li[b], Shu Tao[b], and Dongqiang Zhu[a,b,*]

[a] State Key Laboratory of Pollution Control and Resource Reuse, School of the Environment, Nanjing University, Jiangsu 210046, China

[b] School of Urban and Environmental Sciences, Key Laboratory of the Ministry of Education for Earth Surface Processes, Peking University, Beijing 100871, China

[*]Corresponding author. Tel.: +86 010-62766405. E-mail: zhud@pku.edu.cn (D. Zhu)

https://doi.org/10.5194/acp-2020-110
Preprint. Discussion started: 27 February 2020

Atmospheric Chemistry and Physics Discussions

Abstract

The hygroscopic behavior of black carbon (BC) has a significant impact on global and regional climate change. However, the mechanism and factors controlling the hygroscopicity of BC from different carbon sources are not well understood. Here, we systematically measured the equilibrium and kinetics of water uptake by 15 different BC (10 herb-derived BC, 2 wood-derived BC, and 3 soot) using gravimetric water vapor sorption method combined with in-situ diffuse reflectance infrared Fourier transform spectroscopy (DRIFTS). In the gravimetric analysis, the sorption/desorption equilibrium isotherms were measured under continuous-stepwise water vapor pressure conditions, while the kinetics was measured at a variety of humidity levels obtained by different saturated aqueous salt solutions. The equilibrium water uptake of the BC pool at high relative humidity (> 80%) positively correlated to the dissolved mineral content (0.01–13.0wt%) (R^2 = 0.86, P = 0.0001) as well as the content of the thermogravimetrically analyzed organic carbon (OC_{TGA}, 4.48–15.25wt%) (R^2 = 0.52, P = 0.002) and the alkali-extracted organic carbon (OC_{AE}, 0.14–8.39wt%) (R^2 = 0.80, P = 0.0001). In contrast, no positive correlation was obtained with the content of total organic carbon or elemental carbon. Among the major soluble ionic constituents, chloride and ammonium were each correlated with the equilibrium water uptake at high relative humidity. Compared with the herbal BC and soot, the woody BC had much lower equilibrium water uptake, especially at high relative humidity, likely due to the very low dissolved material content and OC content. The DRIFTS analysis provided generally consistent results at low relative humidity. The kinetics of water uptake (measured by pseudo-second order rate constant) correlated to the content of OC_{TGA} and OC_{AE} as well as the content of chloride and ammonium at low relative humidity (33%), but to the porosity of bulk BC at high relative humidity (94%). This

https://doi.org/10.5194/acp-2020-110
Preprint. Discussion started: 27 February 2020


Atmospheric Chemistry and Physics Discussions

was the first study to show that BC of different types and sources has greatly varying hygroscopic properties.

1. Introduction

Black carbon (BC) refers to a collective term of recalcitrant carbonaceous materials generated from incomplete combustion of biomass and fossil fuels (Bond et al., 2013). BC is ubiquitous in the atmosphere and is a major component of atmospheric carbonaceous aerosols (Schwarz et al., 2008). Due to the strong ability to absorb visible light (Yuan et al., 2015), BC causes positive radiative forcing effects on climate and is considered an important factor driving global warming (Matthews et al., 2009). Once immersed into cloud droplets, BC can also facilitate water evaporation and cloud dispersion via enhanced absorption of solar radiation, and thus produce indirect radiative forcing effects (Powelson et al., 2014). Additionally, the large specific surface area of BC creates a potential for heterogeneous reactions with trace gases (such as volatile halocarbons) in the atmosphere (Qiu et al., 2012), therefore heavily impacting atmospheric chemistry and air quality. Hygroscopicity is a key determinant of physical, chemical, and optical properties of BC by changing particle size, phase state, and quality and morphological development, which in turn affect aerosol radiation effect, formation of cloud and ice nuclei, and heterogeneous chemical reactions (Bond et al., 2013; Liu et al., 2018). Furthermore, the hygroscopicity of BC is an important factor contributing to the risk of human respiratory infections, cardiovascular diseases, and other infectious diseases (Haddrell et al., 2015).

BC is composed of a complex matrix of inorganic and organic components. The inorganic components consist of a variety of amorphous or crystalline salts (sulfates, chlorides, etc.) as well as semi-crystalline minerals (such as silica) (Stanislav et al.,

https://doi.org/10.5194/acp-2020-110
Preprint. Discussion started: 27 February 2020


Atmospheric Chemistry and Physics Discussions

2013). Despite the relatively low content in BC, the inorganic components play a significant role in water uptake of BC, depending on their types, contents, and mixing ratios (Lewis et al., 2009). As the factors and processes governing the hygroscopic deliquescence of inorganic salts are very complicated (Reid et al., 2005; Zhang et al., 2012), it is of a great challenge to assess the contribution of a specific salt to the overall hygroscopicity of BC, and thus, its role is still controversial. Previous studies suggested that KCl was responsible for the high hygroscopicity of BC produced by fresh biomass burning (Posfai et al., 2003), while the presence of K_2SO_4 or KNO_3 caused the low hygroscopicity of BC produced by aged biomass burning (Li et al., 2003).

The organic components in BC consist of graphitized elemental carbon (EC) and non-condensed, amorphous organic carbon (OC) (Lian and Xing, 2017). The contribution of EC to the overall hygroscopicity of BC is considered low due to the very high hydrophobicity (Seisel et al., 2005). The role of OC in the hygroscopic growth of BC is intricate and debatable. The positive effect of OC is mainly attributed to water absorption by the oxygen-containing functional groups (Fletcher et al., 2007; Suda et al., 2014). The negative effect of OC is suggested to stem from the impeded mass transfer process of water molecules by formation of coatings on hygroscopic minerals or inhomogeneous morphology inside the particle (Sjogren et al., 2007; Stemmler et al., 2008). In addition to the total content, the molecular weight, water solubility, surface tension, and type and content of functional groups of OC were all found to influence the overall hygroscopicity of BC. Moreover, the effect of OC on BC hygroscopicity is further complicated by the formation of organic minerals (presumably through strong covalent bonds) (Archanjo et al., 2014; Reid et al., 2005; Zuend et al., 2011).

https://doi.org/10.5194/acp-2020-110
Preprint. Discussion started: 27 February 2020


Atmospheric Chemistry and Physics Discussions

89 The carbon sources for BC particles released into the atmosphere are expected to be
90 highly diversified and cover a wide range of plant biomass, coals, and refined oil
91 products, although their quota can hardly be accurately assessed (Andreae and
92 Gelencser, 2006). The chemical compositional and structural properties of BC depend
93 significantly on carbon sources and combustion conditions (Xiao et al., 2018). For
94 instance, crop residue-derived biochar often has higher mineral content than
95 wood-derived charcoal, while biochar formed at higher pyrolysis temperatures
96 generally have higher aromaticity, specific surface area, and pore volume but lower
97 polarity than biochar formed at lower temperatures (Wei et al., 2019). Previous studies
98 on hygroscopicity of BC have mainly focused on wood-derived BC (Carrico et al.,
99 2010; Day et al., 2006), whereas BC from other carbon sources has been largely
100 overlooked. It remains unclear whether BC from different carbon sources would differ
101 significantly in hygroscopicity.

102 Herein we systematically investigated the equilibrium and kinetics of water uptake
103 by 15 different BC samples derived from wood, herb, coal, and diesel at varying
104 relative humidity (RH) levels by gravimetric sorption and in-situ diffuse reflectance
105 infrared Fourier transform spectroscopy (DRIFTS). The chemical, compositional, and
106 structural properties of the tested BC pool were thoroughly characterized to unveil the
107 key factors controlling the hygroscopic properties.

108 **2. Experimental methods**

109 **2.1. Preparation of BC**

110 A total of 15 BC samples were tested, including 10 herb-derived BC, 2 wood-derived
111 BC, and 3 soot. The herbal BC from amaranth, peanuts, pea, grass, rice, wheat, corn,
112 millet, sorghum, and bamboo, and woody BC from red pine and poplar, respectively
113 were prepared by pyrolysis. Briefly, the dried and dehydrated biomass was pulverized

https://doi.org/10.5194/acp-2020-110
Preprint. Discussion started: 27 February 2020


Atmospheric Chemistry and Physics Discussions

into a fine powder using a high-speed pulverizer (FW 100, Tianjin Taisite Instrument, China), and pyrolyzed in a muffle furnace under an oxygen-limited conditions. The oven temperature was programmed to increase from 20 to 400 °C in 2 h and maintained at 400 °C for 3 h. The Household soot was freshly collected on the inner wall of the stove chamber produced by burning of coal and wood for winter cooking and heating (Linkou County, Heilongjiang Province, China). The Weifu diesel soot produced by burning diesel (# 5, China) at 1000 °C was collected by a diesel particulate filter from the exhaust stream at a carbon deposition temperature of 250 °C. The diesel engine soot was taken from the freshly discharged exhaust particles on the tailpipe of a diesel truck (# 0, 3.7 L, CY4100, Dongfeng, China). The obtained BC and soot samples were further ground to pass a 100-mesh sieve (0.15 mm) and stored sealed in a brown glass bottle at 4 °C.

2.2. Characterization of BC

Elemental analysis (EA) was performed using a Vario micro cube elemental analyzer (Elementar, Hanau, Germany). Surface elemental compositions were measured by X-ray photoelectron spectroscopy (XPS) (PHI 5000 VersaProbe, UlVAC-PHI, Japan). Mineral compositions were measured by X-ray fluorescence (XRF) (ARL-9800, ARL Corporation, Switzerland). Fourier-transform infrared (FTIR) spectra were recorded on a Bruker Tensor 27 Karlsruhe spectrometer (Germany) using KBr pellets in the range of 400 to 4000 cm^{-1}. X-ray diffraction (XRD) spectra were recorded on an AXS D8 Advance spectrometer (Germany) using Cu Kα radiation at a 2θ angle ranging from 5 to 70°. Raman spectra were collected on a Horiba Jobin Yvon LabRam HR-800 spectrometer equipped with a 514 nm laser (France). N_2 adsorption isotherms to the 15 BC were obtained on a Micrometrics ASAP 2020 (Micromeritics Instrument Co., Norcross, GA, USA) apparatus at -196 ºC (77 K).

https://doi.org/10.5194/acp-2020-110
Preprint. Discussion started: 27 February 2020

Atmospheric Chemistry and Physics Discussions

Three different methods, thermogravimetric analysis (TGA), alkali extraction, and water extraction, were explored to quantify the content of OC in BC (referred to as OC_{TGA}, OC_{AE}, and OC_{WE}, respectively). The content of OC_{TGA} was measured as the weight loss during the heating of BC from 30 to 300 °C at a ramp of 10 °C per minute in a nitrogen flow (Han et al., 2013) using a TGA 8000 analyzer (PerkinElmer, USA). To measure the content of OC_{AE}, the BC sample was mixed with 0.1 M NaOH at a solid-to-solution ratio of 1: 10 (w/w) and magnetically stirred for 12 h, followed by filtration through a 0.45-μm filter membrane (Pall, USA) (Song et al., 2002). The procedure was repeated until the filtered supernatant was colorless. The filtrate was collected and the total organic carbon (TOC) content was measured by a TOC analyzer (TOC-5000A, Shimadzu, Japan). For three selected BC (Grass BC, Wheat BC and Household soot), the filtrate was precipitated by acidification (pH 1.0 with 6 M HCl), which was separated by centrifugation and dialyzed in deionized (DI) water by dialysis bag (500 Da, Union Carbide, USA) until no chloride ion was detected by $AgNO_3$, and then freeze-dried. The elemental compositions of the three prepared OC_{AE} were measured by EA. To measure the content of OC_{WE} and dissolved minerals, the BC suspended in DI water (BC-to-water ratio of 1: 10, w/w) was sonicated in a water bath for several minutes, and the mixture was filtered through a 0.45-μm membrane. This procedure was repeated for 6 times. The filtrate was collected and subjected to TOC analysis to obtain the content of OC_{WE}. The concentrations of ionic constituents (Cl^-, NO_3^-, PO_4^{3-}, SO_4^{2-}, F^-, COO^-, $C_2O_4^{2-}$, Na^+, NH_4^+, K^+, Mg^{2+}, Ca^{2+}, Al^{3+}) in the filtrate were measured using a Dionex ICS-1100 ion chromatography (Thermo Scientific, USA). The cations were eluted using 20 mM methanesulfonic acid on a Dionex IonPac CS12A column (4 × 250 mm), while the anions were eluted using an eluent of 4.5 mM Na_2CO_3 and 0.81

https://doi.org/10.5194/acp-2020-110
Preprint. Discussion started: 27 February 2020


Atmospheric Chemistry and Physics Discussions

mM $NaHCO_3$ on a Dionex IonPac AS14A column (4 × 250 mm). The filtrate was further freeze-dried and baked at 600 °C for 6 h to remove organic components. The remaining ash was weighed to determine the content of dissolved minerals in BC. A portion of the ash was extracted three times using DI water at a solid-to-solution ratio of 1:10 (w/w) under sonication, and the salinity of the extract was measured by a ST3100C conductivity meter (OHAUS, USA). All reagents and chemicals used were of analytical reagent grade.

2.3. Measurement of BC hygroscopicity

The hygroscopicity of BC at varying RH was measured by gravimetric method combined with in-situ DRIFTS. The water vapor sorption/desorption isotherms to BC under a range of continuous-stepwise water vapor pressures were acquired on a 3H-2000 PW Multi-stations Gravimetric Method Steam Adsorption Instrument (Beijing, China) at 25 °C using an approach similar to that in previous studies (Gu et al., 2017). The instrument consists of two main parts: a balance chamber to determine the sample mass to an accuracy ±1 μg and a humidity chamber to regulate the water vapor pressure to the desired value as monitored online by a pressure sensor. Prior to testing, the BC sample (about 10 mg) was dried at 70 °C under vacuum for 12 h to remove pre-adsorbed gases. The amount of water sorbed to BC was monitored as the mass difference before and after sorption. The amount of water sorbed to the sample tube was negligible (< 0.05% of the amount of water sorbed to BC). The water vapor pressures ranging from 10 to 94% RH were applied to the sorption isotherm branch in a stepwise increasing sequence and to the desorption isotherm branch in a stepwise decreasing sequence.

The kinetics of water sorption to BC was measured on a 100 mm closed quartz chamber (Jiangsu Province, China) using a gravimetric method similar to that in

https://doi.org/10.5194/acp-2020-110
Preprint. Discussion started: 27 February 2020


Atmospheric Chemistry and Physics Discussions

189 previous studies (Yuan et al., 2014). Approximately 100 mg of BC sample was dried
190 at 70 °C under vacuum for 12 h, weighed in a 10-mL beaker, and placed in a chamber
191 under controlled humidity conditions based on different saturated aqueous salt
192 solutions according to ASTM E104-02 (2007). The saturated solutions of CH_3COOK,
193 $MgCl_2$, K_2CO_3, $LiNO_3$, NaCl, KCl, and KNO_3 provided RH of 23%, 33%, 43%, 47%,
194 75%, 84%, 94%, respectively at 25 °C. The sample was continuously weighed and
195 recorded over a period of time (48 h for low humidity and 96 h for high humidity) to
196 monitor the amount of sorbed water. The RH was monitored in real time using a
197 Honeywell HIH4000 hygrometer (USA) with measurement variance was less than 5%.
198 Sorption equilibrium was reached in the late stage of the experiment as evidenced by
199 the stabilized constant value of sample mass. In addition to kinetic data, sorption
200 isotherms were also collected for the seven selected RH levels using the measured
201 mass under equilibrium conditions.
202 BC samples equilibrated at different RH levels were characterized by in situ
203 DRIFTS using a Bruker Tensor 27 spectrometer equipped with a high-sensitivity
204 mercury-cadmium-telluride (MCT) detector working under liquid N_2 conditions and a
205 chamber fitted with ZnSe windows (Harrick Scientific, USA). About 10 mg of BC
206 pre-dried at 70 °C under vacuum for 12 h was transferred to the chamber which was
207 connected to a gas feeding system. The chamber was sealed and purged with
208 high-purity N_2 at a flow rate of 100 mL per minute for at least 3 h to remove
209 pre-adsorbed gases on BC and to minimize the interference of environmental CO_2.
210 The humidity in the chamber was regulated by mixing high-purity N_2 and saturated
211 water vapor at 25 °C with varying ratios and monitored in real time by a hygrometer
212 (Vaisala Humitter, Australia). The sample was equilibrated with the gas mixture in the
213 chamber for at least 30 minutes to reach sorption equilibrium based on pre-determined

https://doi.org/10.5194/acp-2020-110
Preprint. Discussion started: 27 February 2020


Atmospheric Chemistry and Physics Discussions

kinetics. The spectra were acquired by co-adding and averaging a plurality of 500 scans with a resolution of 4 cm^{-1} (Song and Boily, 2013). The amount of water sorbed to BC was monitored by the integrated intensity of the O-H stretching region from 2750 to 3660 cm^{-1} (Ghorai et al., 2011).

3. Results and discussion

3.1. Characteristics of BC

Bulk elemental compositions by EA and surface elemental compositions by XPS are summarized in Table S1. The bulk elemental compositions of all BC samples were dominated by C and O, together accounting for 54%–96% of the total. However, the bulk C, O compositions differed significantly among the 15 BC, ranging from 32 to 76% for C and from 16 to 69% for O. With the exception of the woody BC, the differences were apparent within each category of the herbal BC and the soot. The surface elemental compositions were also dominated by C and O, but the compositional differences among the 15 BC were much smaller than the bulk elemental compositions. Besides C and O, EA detected low amounts of N (< 3.7%) and S (< 1.8%), and XPS detected low amounts of N (< 4.3%), Si (< 5.6%), and S (< 0.6%). The contents of oxygen-containing groups in the 15 BC were qualitatively compared by the FTIR spectra (Figure S1). All the tested BC except Weifu diesel soot showed characteristic peaks of esters (1700 cm^{-1}), ketones (1613, 1100 cm^{-1}), and phenols (1270 cm^{-1}) (Keiluweit et al., 2010), generally with larger peak intensities observed for herbal-derived BC and household soot.

https://doi.org/10.5194/acp-2020-110
Preprint. Discussion started: 27 February 2020

Atmospheric Chemistry and Physics Discussions

235 Table 1. Chemical, compositional, and pore properties of different BC.

Samples	OC			EC[d]	Dissolved minerals	Total Porosity[e]	SSA[f]
	OC_{TGA}[a] (wt%)	OC_{AE}[b] (wt%)	OC_{WE}[c] (wt%)	(wt%)	(wt%)	(m^3 g^{-1})	(m^2 g^{-1})
Amaranth BC	6.24	2.6	1.75	25.84	10.8	0.004	0.314
Grass BC	7.24	2.37	1.01	51.56	4.8	0.008	5.587
Peanuts BC	7.45	1.78	0.8	41.86	4.2	0.002	0.192
Pea BC	9.59	1.98	0.09	54.48	3.6	0.005	4.679
Rice BC	6.81	0.6	0.11	48.06	0.6	0.023	31.88
Wheat BC	8.25	1.82	0.37	42.65	5.8	0.01	7.382
Millet BC	9.41	1.97	0.93	32.25	8	0.023	8.319
Corn BC	6.55	0.14	0.32	46.47	1.8	0.028	28.6
Sorghum BC	9.09	1.12	0.62	55.26	4.8	0.001	0.192
Bamboo BC	6.84	0.23	0.12	61.7	0.6	0.029	51.94
Red pine BC	7.4	0.2	0.05	62.59	0.01	0.032	64.24
Poplar BC	7.58	0.19	0.09	64.22	0.6	0.071	107.6
Diesel engine soot	9.57	1.4	0.78	27.37	3.6	0.021	6.119
Weifu diesel soot	4.48	0.57	0.13	71.98	3.4	0.484	194.6
Household soot	15.25	8.39	2.24	21.83	13	0.012	7.79

236 [a]Content of organic carbon determined by TGA. [b]Content of alkali-extractedorganic
237 carbondetermined by TOC analysis. [c]Content of water-extracted organic
238 carbondetermined by TOC analysis. [d]Determined by subtracting OC_{TGA} content from
239 total organic carbon content by EA. [e]Total pore volume determined by N_2 adsorption
240 at 0.97 atmosphere pressure. [f]Specific surface area determined by the BET method.

241 Table 1 summarizes the contents of OC (OC_{TGA}, OC_{AE}, and OC_{WE}) of the 15 BC by
242 TGA, alkali extraction, and water extraction, respectively. For a given BC, the
243 contents of the three types of OC differed pronouncedly, with an increasing order of
244 $OC_{WE} < OC_{AE} < OC_{TGA}$. The OC content also differed within the tested BC pool,
245 ranging from 0.05 to 2.24wt% for OC_{WE}, from 0.14 to 8.39wt% for OC_{AE}, and from
246 4.48 to 15.25wt% for OC_{TGA}. Compared with the EC (graphitized carbon), the three
247 types of OC are non-condensed, amorphous, and more rich in oxygen-containing
248 functional groups. This was evidenced by the fact that the OC_{AE} from the three
249 selected BC (Grass BC, Wheat BC and Household soot) had markedly higher bulk

https://doi.org/10.5194/acp-2020-110
Preprint. Discussion started: 27 February 2020


Atmospheric Chemistry and Physics Discussions

compositions of O (results presented in Table S2). The content of EC in BC was roughly assessed by subtracting the OC_{TGA} content from the total organic carbon content measured by EA (results presented in Table 1). The calculated EC content negatively correlated with the OC_{AE} content (R^2 = 0.43, P = 0.0079) for the examined BC pool. This was reasonable as EC was comprised of mature, thermodynamically stable graphitized carbons, while OC was comprised of the less mature and less aromatic constituents remaining after pyrolysis. Except for Weifu diesel soot, the two woody BC had the highest EC, but the lowest OC_{AE} and OC_{WE} among the 15 BC.

The relative abundance of EC in BC was also assessed by Raman spectroscopy (Figure S2). The spectra of all the tested BC were dominated by a D band at 1340 cm^{-1} and a G band at 1580 cm^{-1}, which were ascribed to carbon network defects and the E_{2g} mode of the graphitized carbon, respectively (Pimenta et al., 2007). Thus, the ratio of these two bands (I_D/I_G) was inversely proportional to the in-plane crystallite size of graphitized carbons of BC (Cancado et al., 2006). The I_D/I_G ratio of the woody BC (0.51–0.59) was less than those of the herbal BC (0.88–1.09) and the soot (0.77–1.12) (Table S3), suggesting larger sizes of graphitized carbons in the woody BC. This was consistent with the results of OC compositions.

The contents of dissolved minerals of the 15 BC are listed in Table 1, and their salinities in water extracts are listed in Table S4. The two woody BC had the lowest contents of dissolved minerals and salinities, while these contents in herbal BC and soot were higher and varied greatly. The mineral compositions characterized by XRF are listed in Table S5. Si-, K-rich minerals were the two major inorganic constituents in the herbal BC and woody BC. Moreover, these two types of BC generally contained trace amounts of S-, Cl-, Ca-, P-, Mg-, Na-, Fe-, and Al-minerals, with lower contents observed for the woody BC. The three soot had very different mineral

https://doi.org/10.5194/acp-2020-110
Preprint. Discussion started: 27 February 2020


Atmospheric Chemistry and Physics Discussions

compositions. Household soot was dominated by S-, Ca-, Si, and Cl-minerals, Diesel engine soot was dominated by S-, Ca-, and Fe-minerals, while Weifu diesel soot contained negligible mineral compositions. As reflected by the observed characteristic peaks and associated peak intensities in the XRD spectra (Figure S3), the herbal BC and Household soot contained more mineral species with higher contents than other BC, whereas the two woody BC and Weifu diesel soot contained the least species and contents of minerals. Potassium salts, amorphous silica, and sulfates were the major minerals in the herbal BC. Soot had the largest content of sulfates among the tested BC. According to the ion chromatograph analysis (results presented in Figure S4 and Table S6), the major water-extracted cationic species from the tested BC were NH_4^+, K^+, and Ca^{2+}, and the major anionic species were SO_4^{2-}, Cl^-, and $C_2O_4^{2-}$. The herbal BC had high contents of K^+, $C_2O_4^{2-}$, and Cl^-, while the soot had high content of SO_4^{2-}.

The Brunauer–Emmett–Teller (BET) specific surface area and total porosity measured by N_2 adsorption are also summarized in Table 1. A huge disparity of specific surface area was shown among the 15 BC and among the BC within each category, ranging from 6 to 200 $m^2\ g^{-1}$ for the soot, from 60 to 110 $m^2\ g^{-1}$ for the woody BC, and from 0.1 to 52 $m^2\ g^{-1}$ for the herbal BC. The herbal BC and woody BC were dominated by micropores (pore size < 2 nm), which accounted for more than 50% of the total pore volume. Alternatively, mesopores (50 nm > pore size > 2 nm) were the main pore structure of the soot, accounting for more than 61% of the total pore volume.

3.2. Hygroscopic properties of BC

Equilibrium water uptake. Figure 1 displays sorption and desorption isotherms of water vapor with BC plotted as equilibrium water uptake (mg g^{-1}) by unit mass of BC under continuous-stepwise water vapor pressure conditions. Figure S5 displays the

https://doi.org/10.5194/acp-2020-110
Preprint. Discussion started: 27 February 2020

Atmospheric Chemistry and Physics Discussions

equilibrium sorption isotherms at selected humidity levels obtained by using saturated aqueous salt solutions. Under similar humidity conditions (80% and 84%), the water uptake by the 15 BC was very close between these two humidity regulation methods (Figure S6), reflecting their technical validity. The woody BC showed very different sorption isotherm patterns from the herbal BC and soot. First, the water sorbing ability of the woody BC was much lower. The maximum water uptake observed at the highest RH (94%) was approximately 65 mg g^{-1} by the woody BC, but was more than 400 mg g^{-1} for the strongest sorbing herbal BC and soot. Second, much larger water-uptake disparities were observed within the herbal BC group and the soot group than within the woody BC group. Additionally, over the examined RH range (10–94%), the water uptake by the woody BC increased slowly and linearly with the RH; however, for the herbal BC and soot, the water uptake increased more rapidly with the RH, especially under high humidity conditions (RH > 70%).

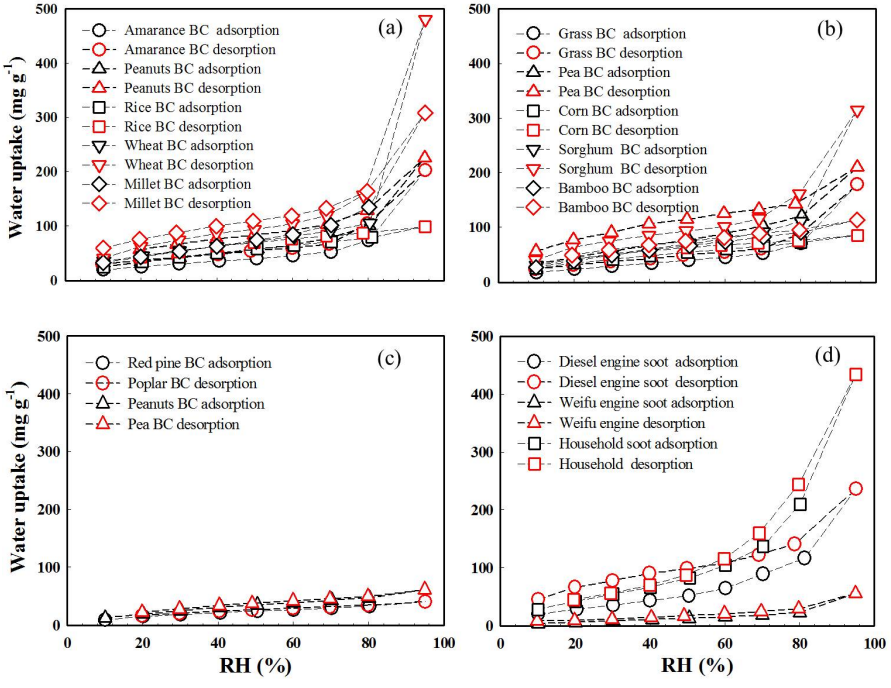

https://doi.org/10.5194/acp-2020-110
Preprint. Discussion started: 27 February 2020


Atmospheric Chemistry and Physics Discussions

Figure 1. Sorption and desorption isotherms of water vapor plotted as water uptake (mg g^{-1}) vs. relative humidity (RH, %) at equilibrium for different BC. (a) Subgroup 1 of herbal BC. (b) Subgroup 2 of herbal BC. (c) Woody BC. (d) Soot.

To better understand the underlying mechanisms and factors controlling the hygroscopic properties of BC, linear relationships were built between the equilibrium water uptake and a wide variety of compositional and pore property parameters of the whole BC pool. Figure 2 displays regression relationships with contents of OC_{TGA}, OC_{AE}, EC, dissolved minerals, major ionic species (NH_4^+, Cl^-, SO_4^{2-}, and $C_2O_4^{2-}$), and total porosity, respectively at 94% RH. The regression relationships at 23% RH were presented in Figure S7. The regression accuracy (R^2 and P) values at the 7 different RH levels ranging from 23% to 94% are summarized in Table S7. Good positive correlations existed between the water uptake and the contents of OC_{TGA}, OC_{AE}, and dissolved minerals under high humidity conditions (Figure 2a-d). The highest regression accuracy values obtained were $R^2 = 0.82$, $P < 0.0001$ for OC_{TGA} at 84% RH, $R^2 = 0.80$, $P = 0.001$ for OC_{AE} at 94% RH, and $R^2 = 0.86$, $P = 0.0001$ for dissolved minerals at 94% RH. However, the correlations with these BC constituents became much weaker under low humidity conditions ($R^2 = 0.10–0.32$, $P = 0.247–0.028$ at RH = 23%). It can be concluded that the hygroscopicity of herbal BC and soot under high humidity conditions was mainly controlled by the contents of OC and dissolved minerals. On the other hand, the low water sorbing ability of the woody BC was due to the very low contents of these constituents. The OC constituents in BC contained large amounts of oxygen-containing groups and thus had very high hygroscopicity (Xiao et al., 2013). The very strong water retention ability of dissolved minerals in BC was understandable due to the strong hydration of mineral surfaces and ionic constituents. No correlation was observed between the water uptake of BC

https://doi.org/10.5194/acp-2020-110
Preprint. Discussion started: 27 February 2020

Atmospheric Chemistry and Physics Discussions

339 and the total organic carbon content within the whole examined RH range. Notably, a
340 negative correlation was observed with the EC content (Figure 2c), especially under
341 high humidity conditions (R^2 = 0.54, P = 0.0019 at 94% RH). Compared with the OC
342 in BC, the EC was comprised mainly of hydrophobic fuse aromatic hydrocarbons and
343 had much lower amounts of oxygen-containing groups, resulting in the very low water
344 sorbing ability.

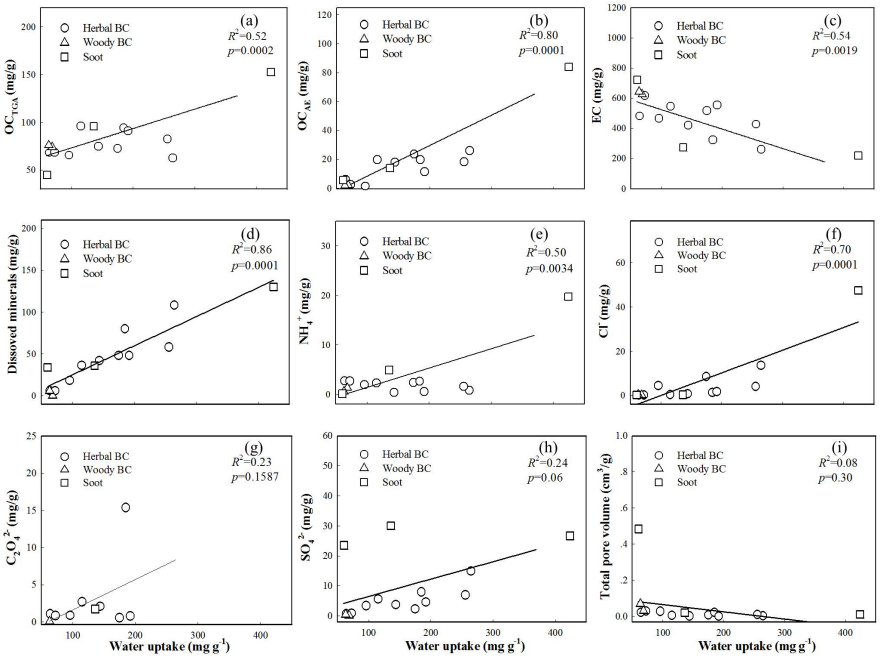

345

346 Figure 2. Relationships between equilibrium water uptake (mg g^{-1}) vs. compositional
347 and pore property parameters for the BC pool at 94% relative humidity. (a)
348 TGA-measured organic carbon (OC_{TGA}). (b) Alkali-extracted organic carbon (OC_{AE}).
349 (c) Elemental carbon (EC). (d) Dissolved minerals. (e) Ammonium (NH_4^+). (f)
350 Chloride (Cl^-). (g) Oxalate ($C_2O_4^{2-}$). (h) Sulfate (SO_4^{2-}). (i) Total porosity.

351 At 94% RH, relatively good positive correlations were observed with NH_4^+ and Cl^-
352 (R^2 = 0.50–0.70, P = 0.0001–0.0034), but not with SO_4^{2-} (R^2 = 0.24, P = 0.06) or

https://doi.org/10.5194/acp-2020-110
Preprint. Discussion started: 27 February 2020


Atmospheric Chemistry and Physics Discussions

353 $C_2O_4^{2-}$ (R^2 = 0.23, P = 0.1587) (Figure 2e-h). No correlation (R^2 = 0.08, P = 0.3) was
354 observed with the total porosity of BC at 94% RH (Figure 2i). Consistently, previous
355 studies reported that chloride salts in biomass burning aerosols had high
356 hygroscopicity (Jing et al., 2017; Posfai et al., 2003). The poor correlation observed
357 for SO_4^{2-} was ascribed to the low hygroscopicity of $CaSO_4$ and K_2SO_4, as evidenced
358 by their very high deliquescent relative humidity (96–97%) (Freney et al., 2007;
359 Preturlan et al., 2019). It is noteworthy that the content of SO_4^{2-} positively correlated
360 with the contents of Ca^{2+} (R^2 = 0.74, P $<$ 0.0001) and K^+ (R^2 = 0.69, P = 0.0008) for
361 the tested BC. On the other hand, the poor correlation observed for $C_2O_4^{2-}$ was likely
362 due to the formation of less water-soluble salts (e.g., $K_2C_2O_4$) that might depress the
363 hygroscopicity (Buchholz and Mentel, 2008).

364 The positive correlations observed with NH_4^+ and Cl^- at 94% RH disappeared at
365 23% RH. Alternatively, a relative good negative correlation (R^2 = 0.42, P = 0.0095)
366 with the total porosity was shown at 23% RH (Figure S7i). Similarly, a weak negative
367 correlation (R^2 = 0.21, P = 0.083) was shown with the EC content at 23% RH. On the
368 contrary, a weak positive correlation (R^2 = 0.32, P = 0.028) was observed between the
369 water uptake and the OC_{TGA} content. It was reasonable to hypothesize that the rigid
370 micro- and mesoporous structures in BC were mainly formed by graphitized carbons
371 (EC) rather than by amorphous organic carbons (OC). Thus, the abovementioned
372 correlations indicated that the OC constituents played a key role in the overall water
373 uptake by BC under low humidity conditions.

374 As can be seen from the desorption isotherms in Figure 1, the herbal BC and soot
375 showed certain hysteresis effect (irreversible sorption), whereas the woody BC
376 showed no hysteresis effect. Irreversible sorption would lower the release of sorbed
377 water molecules from BC particles in the atmosphere when the RH changes from a

https://doi.org/10.5194/acp-2020-110
Preprint. Discussion started: 27 February 2020


Atmospheric Chemistry and Physics Discussions

high level to a low level. The observed hysteresis effect of herbal BC and soot likely stemmed from their relatively high contents of OC and/or dissolved minerals (such as wheat BC and Household soot). Sorbing water molecules could cause strong and irreversible hydration of organic acids (Petters et al., 2017) and dissolution or phase change of minerals (Adapa et al., 2018), consequently leading to hysteresis effect due to non-identical structures of BC between the sorption and desorption branches even at the same RH. The negligible hysteresis effect observed on the two woody BC could be attributed to their very low contents of OC and dissolved minerals.

The equilibrium water uptake by BC was further investigated by DRIFTS. The spectra of representative BC (Grass BC, Red pine BC, and Household soot) at varying RH are presented in Figure 3a-c. Figure 3d compares the water uptake at 23% RH monitored by the integrated intensity of the O-H stretching region from 2750 to 3660 cm^{-1} (Ghorai et al., 2011), along with the water uptake measured by the multi-station gravimetric method for 8 selected BC. The identified bands of sorbed water molecules included a combination mode of symmetric stretch around 3423 cm^{-1} and asymmetric stretch stretch around 3253 cm^{-1} (Gustafsson et al., 2005). The broad feature peak centered at 2100 cm^{-1} was assigned to a combined band of bending, libration, and hindered translation modes of water, while the peak centered at 1640 cm^{-1} was attributed to the bending mode of water (Ma et al., 2010). The intensities of these peaks/bands increased with increasing RH. As assessed by the integrated intensity of the O-H stretching region (see insets in Figure 3a-c), the water uptake by Grass BC and Household soot increased gradually with RH from 12 to 80%; however, the water uptake by Red pine BC rapidly reached saturation at about 28% RH, and kept constant when the RH was further increased. With the exception of Weifu diesel soot, the disparity pattern of water uptake by the 8 selected BC at 23% RH monitored

https://doi.org/10.5194/acp-2020-110
Preprint. Discussion started: 27 February 2020

Atmospheric Chemistry and Physics Discussions

by DRIFTS was similar to that monitored by the multi-station gravimetric method (Figure 3d). However, the disparities were very large between these two methods at 80% RH (Figure S8). This was probably because the saturated effect encountered in detection of sorbed water molecules by FTIR (Gustafsson et al., 2005) became worse under high humidity conditions. Moreover, the DRIFTS signals of sorbed water molecules might be influenced by the distribution of sorption sites (e.g., minerals vs. OC and exterior vs. interior), and the caused effects might lead to larger deviations under high humidity conditions.

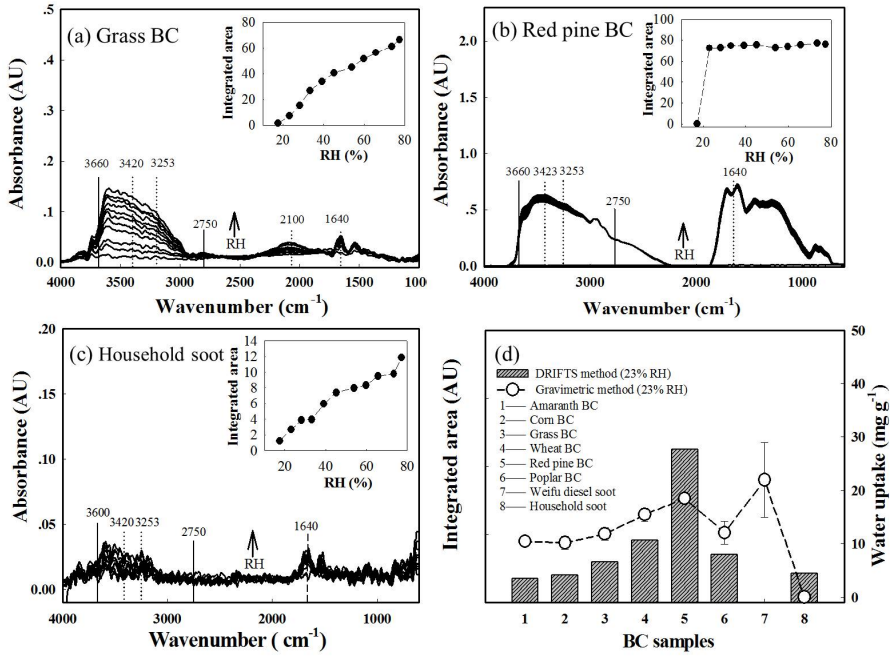

Figure 3. Diffuse reflectance infrared Fourier transform spectroscopy (DRIFTS) characterization of equilibrium water uptake by BC. (a-c) Spectra for three representative BC (Grass BC, Red pine BC, and Household BC) equilibrated at varying relative humidity (RH) levels. (d) Comparison of equilibrium water uptake measured as integrated area of O-H stretching region (2750–3660 cm^{-1}) between 8

https://doi.org/10.5194/acp-2020-110
Preprint. Discussion started: 27 February 2020


Atmospheric Chemistry and Physics Discussions

417 selected BC at 23% relative humidity. Insets in subfigures (a-c) present water uptake
418 measured as integrated area of O-H stretching region against RH.

419 **Kinetic water uptake.** Figure 4 displays the water vapor sorption kinetics to the 15
420 BC at 94% RH obtained by saturated aqueous salt solutions. The sorption kinetics at
421 33% RH was presented in Figure S9. The two woody BC exhibited similar kinetics
422 curves; however, the herbal BC and soot showed very different kinetic patterns within
423 each group. For quantitative comparison of apparent sorption kinetics among different
424 BC, the data were fitted to the pseudo-first order and pseudo-second order models,
425 $dq_t/dt = k_1 (q_e-q_t)$ and $dq_t/dt = k_2 (q_e-q_t)^2$, respectively, where q_t was the sorbed
426 concentration at time t, q_e was the equilibrium sorbed concentration, and k_1 and k_2
427 were the pseudo-first and pseudo-second rate constants, respectively. The fitting
428 parameters (q_e k_1, k_2) for the three selected RH levels (33, 47, and 94%) are
429 summarized in Table S8-S9 The pseudo-second order model ($R^2 > 0.97$) fits the data
430 better than the pseudo-first order model ($R^2 = 0.80–0.99$). The calculated k_2 differed
431 greatly among the BC within the herbal BC group and the soot group, but was very
432 close between the two woody BC. For a given BC, the k_2 at a lower RH level was
433 significantly larger than that at a higher RH level. Similar results were reported in
434 previous studies on sorption kinetics of water vapor to activated carbon (Ohba and
435 Kaneko, 2011; Ribeiro et al., 2008). Under low humidity conditions, sorption of water
436 vapor mainly occurs at the active, high-energy binding sites, and the sorption kinetics
437 is fast; alternatively, under high humidity conditions, sorption is governed by the slow
438 pore-filling/condensation process of water molecules within the pores of activated
439 carbon via formation of water clusters around the water molecules already sorbed at
440 the active sites (Nguyen and Bhatia, 2011; Rosas et al., 2008). Due to the small
441 molecular size (0.0958 × 0.151 nm, ChemDraw 3D), water molecules could well

https://doi.org/10.5194/acp-2020-110
Preprint. Discussion started: 27 February 2020

Atmospheric Chemistry and Physics Discussions

442 penetrate into the micropores of BC and form water clusters via intermolecular
443 hydrogen bonding. The sorbing ability order of the different types of BC varied
444 depending on the examined RH. At 33% RH, the k_2 roughly followed a decreasing
445 order of soot (0.5–5.25 × 10^{-5} g $mg^{-1}s^{-1}$) > woody BC (1.57–1.90 × 10^{-5} g $mg^{-1}s^{-1}$) >
446 herbal BC (0.34–2.07 × 10^{-5} g $mg^{-1}s^{-1}$); however, no clear trend was shown for high
447 humidity conditions (e.g., RH = 94%), mainly resulting from the larger variances
448 within the herbal BC group and soot group.

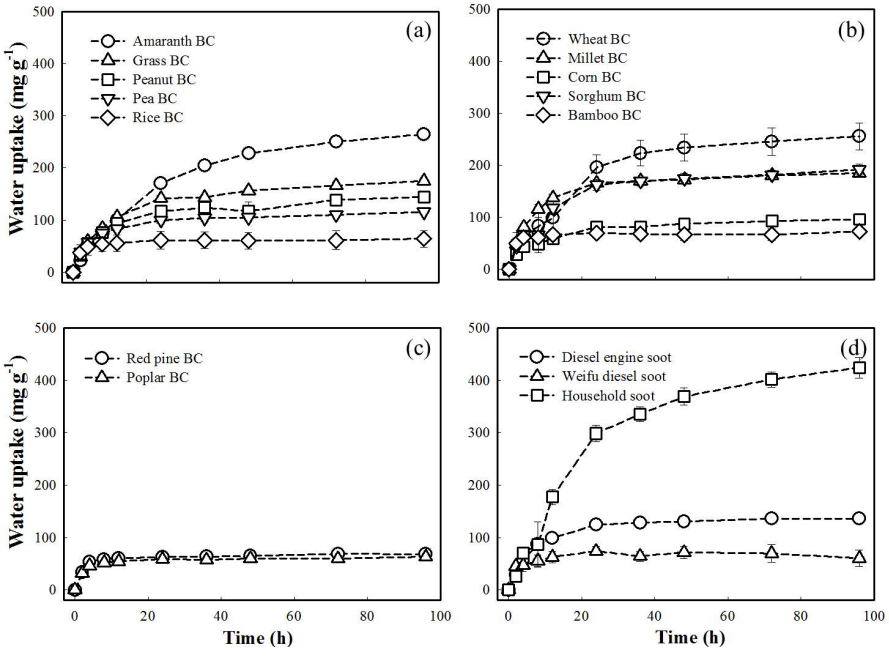

449

450 Figure 4. Sorption kinetics of water vapor plotted as water uptake (mg g^{-1}) vs. time (h)
451 at 94% relative humidity. (a) Subgroup 1 of herbal BC. (b) Subgroup 2 of herbal BC.
452 (c) Woody BC. (d) Soot.

453 Like for the equilibrium water uptake, the relationships were built between the k_2
454 and the contents of OC_{TGA}, OC_{AE}, EC, dissolved minerals, major ionic species (NH_4^+,
455 Cl^-, $C_2O_4^{2-}$ and SO_4^{2-}), and total porosity, respectively at 94% RH (Figure 5). The

https://doi.org/10.5194/acp-2020-110
Preprint. Discussion started: 27 February 2020


Atmospheric Chemistry and Physics Discussions

regression relationships at 33% RH were presented in Figure S10. The regression accuracy (R^2 and P) values at 33%, 47%, and 94% RH are summarized in Table S10. At 94% RH, among the examined parameters only totally porosity was positively correlated with the k_2 (R^2 = 0.82, $P < 0.0001$). This correlation disappeared under low and medium humidity conditions. The strong positive correlation between k_2 and total porosity at high RH can be well explained by the pore-filling/condensation mechanism. A similar mechanism has been previously proposed to account for the positive correlation observed between the water vapor sorption kinetics and the porosity of activated carbon under high humidity conditions (Nakamura et al., 2010; Velasco et al., 2016). At 33% RH, relatively good positive correlations were observed with the contents of OC_{TGA} (R^2 = 0.47, P = 0.0046), OC_{AE} (R^2 = 0.44, P = 0.007), NH_4^+ (R^2 = 0.77, $P < 0.0001$), and Cl^- (R^2 = 0.60, P = 0.0007), but not with $SO4^{2-}$ (R^2 = 0.11, P = 0.2286) or dissolved minerals (R^2 = 0.08, P = 0.31). The positive correlations with these constituents were not shown under medium and high humidity conditions. Thus, the constituents of OC and NH_4^+- and Cl^--salts likely provided the primary high affinity, active sites for sorption of water vapor under low humidity conditions.

https://doi.org/10.5194/acp-2020-110
Preprint. Discussion started: 27 February 2020

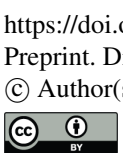

Atmospheric Chemistry and Physics Discussions

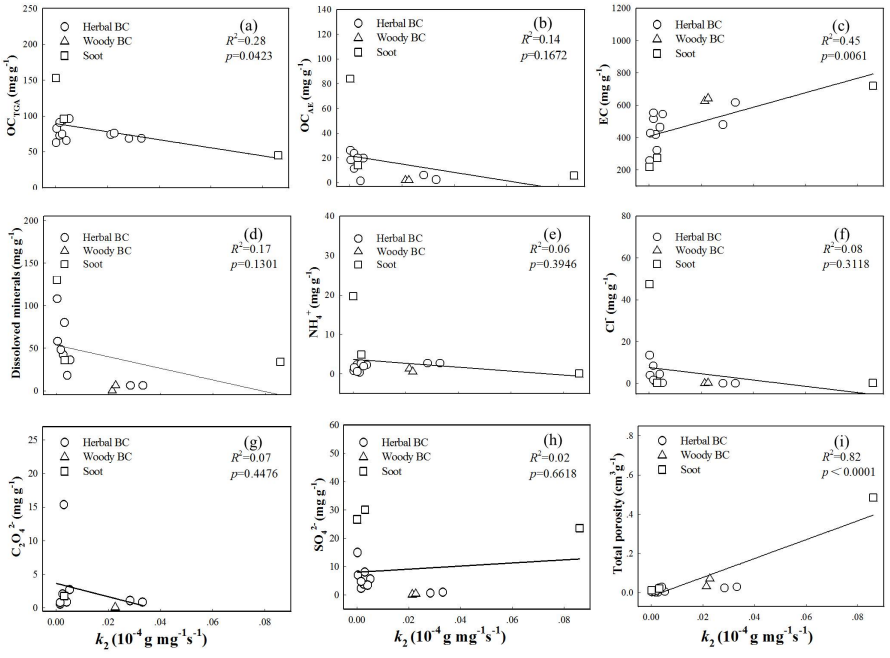

Figure 5. Relationships between pseudo-second water uptake rate constant (k_2) (g mg^{-1}s^{-1}) vs. compositional and pore property parameters for the BC pool at 94% relative humidity. (a) TGA-measured organic carbon (OC_{TGA}). (b) Alkali-extracted organic carbon (OC_{AE}). (c) Elemental carbon (EC). (d) Dissolved minerals. (e) Ammonium (NH_4^+). (f) Chloride (Cl^-). (g) Oxalate ($C_2O_4^{2-}$). (h) Sulfate (SO_4^{2-}). (i) Total porosity.

4. Conclusion

The hygroscopic properties of 15 different BC (herbal, woody, and soot) were systematically investigated using gravimetric method and DRIFTS. The mechanisms and factors controlling the equilibrium and kinetic water uptake differed among the types of BC and depended heavily on the humidity conditions. Linear correlation analyses indicated that the equilibrium water uptake by the tested BC pool positively correlated to the contents of OC (OC_{TGA} and OC_{AE}), dissolved minerals, and NH_4^+- and Cl^--salts under high humidity conditions, and weakly to the contents of OC only

https://doi.org/10.5194/acp-2020-110
Preprint. Discussion started: 27 February 2020


Atmospheric Chemistry and Physics Discussions

under low humidity conditions. By contrast, negative correlations were observed between the equilibrium water uptake and the EC content. The low water uptake by the woody BC could be attributed to the very low contents of OC and dissolved minerals. Thus, the equilibrium water uptake by BC was mainly controlled by the hygroscopic constituents of OC and dissolved minerals/salts. The kinetic water uptake by the BC could be well described by the pseudo-second order kinetic model. The calculated rate constant (k_2) positively correlated to the contents OC_{TGA}, OC_{AE}, and NH_4^+- and Cl^--salts under low humidity conditions, and to the total porosity only under high humidity conditions. The fast water uptake kinetics under low humidity conditions was attributed to the binding to high affinity, active sites (OC and salts), whereas the slow water uptake kinetics under high humidity conditions was attributed to pore-filling/condensation of water molecules within the micro- and mesopores of BC. This study highlights that the hygroscopic properties of BC rely on compositional and structural properties of BC as well as humidity conditions.

Author contributions. DZ provided the original idea and prepared the paper with contributions from all co-authors. MW and YC designed and conducted the research, HF, XQ were involved in the development of the analysis methods. BL, ST reviewed the written document.

Competing interests. The authors declare that they have no conflict of interest.

Acknowledgments. This work was supported by the National Natural Science Foundation of China (Grants 21777002, 21920102002, and 41991331).

Appendix A.

Detailed characterization results of the different BC can be found in Table S1-S5. Table S6 lists accuracy (R^2 and P) values for regression on equilibrium water uptake against different variables. Table S7-S8 presents pseudo-first/second order kinetic

https://doi.org/10.5194/acp-2020-110
Preprint. Discussion started: 27 February 2020


Atmospheric Chemistry and Physics Discussions

model fitting parameters. Table S9 lists accuracy (R^2 and P) values for regression on k_2 against different variables. Figure S1-S4 displays spectroscopic characterization of different BC. Figure S5 displays sorption isotherms at selected humidity obtained by using saturated aqueous salt solutions. Figure S6 compares equilibrium water uptake measured by the two different gravimetric methods. Figure S7 displays relationships between equilibrium water uptake and different variables at 23% RH. Figure S8 compares equilibrium water uptake measured by DRIFTS and gravimetric method at high RH. Figure S9 displays sorption kinetics of water uptake at 33% RH. Figure S10 displays relationships between k_2 and different variables at 33% RH.

https://doi.org/10.5194/acp-2020-110
Preprint. Discussion started: 27 February 2020

Atmospheric Chemistry and Physics Discussions

References

Adapa, S., Swamy, D. R., Kancharla, S., Pradhan, S., and Malani, A.: Role of mono- and divalent surface cations on the structure and adsorption behavior of water on mica surface, Langmuir, 34 (48), 2018.

Andreae, M. O., and Gelencser, A.: Black carbon or brown carbon? The nature of light-absorbing carbonaceous aerosols, Atmos. Chem. Phys., 6, 3131–3148, 2006.

Archanjo, B. S., Araujo, J. R., Silva, A. M., Capaz, R. B., Falcao, N. P. S., Jorio, A., and Achete, C. A.: Chemical analysis and molecular models for calcium-oxygen-carbon interactions in black carbon found in fertile Amazonian anthrosoils, Environ. Sci. Technol., 48, 7445–7452, 2014.

Bond, T. C., Doherty, S. J., Fahey, D. W., Forster, P. M., Berntsen, T., DeAngelo, B. J., Flanner, M. G., Ghan, S., Kärcher, B., Koch, D., Kinne, S., Kondo, Y., Quinn, P. K., Sarofim, M. C., Schultz, M. G., Schulz, M., Venkataraman, C., Zhang, H., Zhang, S., Bellouin, N., Guttikunda, S. K., Hopke, P. K., Jacobson, M. Z., Kaiser, J. W., Klimont, Z., Lohmann, U., Schwarz, J. P., Shindell, D., Storelvmo, T., Warren, S. G., and Zender, C. S.: Bounding the role of black carbon in the climate system: A scientific assessment, J. Geophys. Res. Atmos., 118, 5380–5552, 2013.

Buchholz, A., and Mentel, T. F.: Hygroscopic growth of oxalic acid and its ammonium, sodium and potassium salts, Geophys. Res. Abs., 10, EGU2008-A-03795.

Cancado, L. G., Takai, K., Enoki, T., Endo, M., Kim, Y. A., and Mizusaki, H.: General equation for the determination of the crystallite size L-a of nanographite by Raman spectroscopy, Appl. Phys. Lett., 88 (16), 2006.

Carrico, C. M., Petters, M. D., Kreidenweis, S. M., Sullivan, A. P., McMeeking, G. R., Levin, E. J. T., Engling, G., Malm, W. C., and Collett Jr. J. L.: Water uptake and chemical composition of fresh aerosols generated in open burning of biomass,

https://doi.org/10.5194/acp-2020-110
Preprint. Discussion started: 27 February 2020

547 Atmos. Chem. Phys., 10, 5165–5178, 2010.

548 Day, D. E., Hand, J. L., Carrico, C. M., Engling, G., and Malm, W. C.: Humidification
549 factors from laboratory studies of fresh smoke from biomass fuels, J. Geophys. Res.,
550 111, D22202, 2006.

551 Fletcher, A. J., Uygur, Y., and Mark Thomas, K.: Role of surface functional groups in
552 the adsorption kinetics of water vapor on microporous activated carbons, J. Phys.
553 Chem. C., 111, 8349–8359, 2007.

554 Freney, E. J., Martin, S. T., and Buseck, P. R.: Deliquescence measurements of
555 potassium salts, American Geophysical Union, Fall Meeting, 2007.

556 Ghorai, S., Laskin, A., and Tivanski, A. V.: Spectroscopic evidence of keto-enol
557 tautomerism in deliquesced malonic acid particles, J. Phys. Chem. A., 115,
558 4373–4380, 2011.

559 Gu, W., Li, Y., Zhu, J., Jia, X., Lin, Q., Zhang, G., Ding, X., Song, W., Bi, X., Wang,
560 X., and Tang, M.: Investigation of water adsorption and hygroscopicity of
561 atmospherically relevant particles using a commercial vapor sorption analyzer,
562 Atmos. Meas. Tech., 10, 3821–3832, 2017.

563 Gustafsson, R. J., Orlov, A., Badger, C. L., Griffiths, P. T., Cox, R. A., and Lambert, R.
564 M.: A comprehensive evaluation of water uptake on atmospherically relevant
565 mineral surfaces: DRIFT spectroscopy, thermogravimetric analysis and aerosol
566 growth measurements, Atmos. Chem. Phys., 5, 3415–3421, 2005

567 Haddrell, A. E., Davies, J. F., and Reid, J. P.: Dynamics of particle size on inhalation
568 of environmental aerosol and impact on deposition fraction, Environ. Sci. Technol.,
569 49, 14512–14521, 2015.

570 Han, C., Liu, Y., and He, H.: Role of organic carbon in heterogeneous reaction of NO_2
571 with soot, Environ. Sci. Technol., 47, 3174–3181, 2013.

https://doi.org/10.5194/acp-2020-110
Preprint. Discussion started: 27 February 2020

572 Jing, B., Peng, C., Wang, Y., Liu, Q., Tong, S., Zhang, Y., and Ge, M.: Hygroscopic
573 properties of potassium chloride and its internal mixtures with organic compounds
574 relevant to biomass burning aerosol particles, Sci. Rep., 2, 43573, 2017.
575 Keiluweit, M., Nico, P. S., Johnson, M. G., Kleber, M.: Dynamic molecular structure
576 of plant biomass-derived black carbon (biochar), Environ. Sci. Technol., 44 (4),
577 1247–1253, 2010.
578 Lewis, K. A., Arnott, W. P., Moosmuller, H., Chakrabarty, R. K., Carrico, C. M. ,
579 Kreidenweis, S. M., Day, D. E., Malm, W. C., Laskin, A., Jimenez, J. L., Ulbrich, I.
580 M., Huffman, J. A., Onasch, T. B., Trimborn, A., Liu, L., and Mishchenko, M. I.:
581 Reduction in biomass burning aerosol light absorption upon humidification: roles
582 of inorganically-induced hygroscopicity, particle collapse, and photoacoustic heat
583 and mass transfer, Atmos. Chem. Phys., 9, 8949–8966, 2009.
584 Li, J., Posfai, M., Hobbs, P. V., and Buseck, P. R.: Individual aerosol particles from
585 biomass burning in southern Africa: 2. Compositions and aging of inorganic
586 particles, J. Geophys. Res., 108, 8484, 2003.
587 Lian, F., and Xing, B.: Black carbon (biochar) in water/soil environments: Molecular
588 structure, sorption, stability, and potential risk, Environ. Sci. Technol., 51,
589 13517–13532, 2017.
590 Liu, P., Song, M., Zhao, T., Gunthe, S. S., Ham, S., He, Y., Qin, Y. M., Gong, Z.,
591 Amorim, J. C., Bertram, A. K., and Martin, S. T.: Resolving the mechanisms of
592 hygroscopic growth and cloud condensation nuclei activity for organic particulate
593 matter, Nat. Commun., 9, 4076, 2018.
594 Ma, Q., He, H., Liu, Y.: In situ DRIFTS study of hygroscopic behavior of mineral
595 aerosol, J. Environ. Sci., 22(4), 555–560, 2010.
596 Matthews, H. D., Gillett, N. P., Stott, P. A., and Zickfeld, K.: The proportionality of

https://doi.org/10.5194/acp-2020-110
Preprint. Discussion started: 27 February 2020


Atmospheric Chemistry and Physics Discussions

global warming to cumulative carbon emissions, Nature, 459, 829–832, 2009.

Nakamura, M., Ohba, T., Branton, P., Kanoh, H., and Kaneko, K.: Equilibrium-time and pore width dependent hysteresis of water adsorption isotherm on hydrophobic microporous carbons, Carbon, 48, 2549–2553, 2010.

Nguyen, T. X., and Bhatia, S. K.: How water adsorbs in hydrophobic nanospaces, J. Phys. Chem. C, 115, 16606–16612, 2011.

Ohba, T., and Kaneko, K.: Kinetically forbidden transformations of water molecular assemblies in hydrophobic micropores, Langmuir, 27, 7609–7613, 2011.

Petters, S. S., Pagonis, D., Claflin, M. S., Levin, E. J. T., Petters, M. D., Ziemann, P. J., and Kreidenweis, S. M.: Hygroscopicity of organic compounds as a function of carbon chain length and carboxyl, hydroperoxy, and carbonyl functional groups, J. Phys. Chem. A.J. Phys. Chem. A., 121 (27), 5164–5174, 2017.

Pimenta, M. A., Dresselhaus, G., Dresselhaus, M. S., Cancado, L. G., Jorio, A., and Saito, R.: Studying disorder in graphite-based systems by Raman spectroscopy, Phys. Chem. Chem. Phys., 9, 1276–1291, 2007.

Posfai, M., Simonics, R., Li, J., Hobbs, P. V., and Buseck, P. R.: Individual aerosol particles from biomass burning from southern Africa: 1. Compositions and size distributions of carbonaceous particles, J. Geophys. Res., 108, 8483, 2003.

Powelson, M. H., Espelien, B. M., Hawkins, L. N., Galloway, M. M., and De Haan, D. O.: Brown carbon formation by aqueous-phase carbonyl compound reactions with amines and ammonium sulfate, Environ. Sci. Technol., 48, 985–993, 2014.

Preturlan, J. G. D., Vieille, L., Quiligotti, S., and Favergeon, L.: Comprehensive thermodynamic study of the calcium sulfate–water vapor system. Part 1: experimental measurements and phase equilibria, Ind. Eng. Chem. Res., 58, 22, 9596–9606, 2019.

https://doi.org/10.5194/acp-2020-110
Preprint. Discussion started: 27 February 2020

Atmospheric Chemistry and Physics Discussions

622 Qiu, C., Khalizov, A. F., and Zhang, R.: Soot aging from OH-Initiated oxidation of
623 toluene, Environ. Sci. Technol., 46, 9464−9472, 2012.
624 Reid, J. S., Koppmann, R., Eck, T. F., and Eleuterio, D. P.: A review of biomass
625 burning emissions part II: intensive physical properties of biomass burning particles,
626 Atmos. Chem. Phys., 5, 799–825, 2005.
627 Ribeiro, A. M., Sauer, T. P., Grande, C. A., Moreira, R. F. P. M., Loureiro, J. M., and
628 Rodrigues, A. E.: Adsorption equilibrium and kinetics of water vapor on different
629 adsorbents, Ind. Eng. Chem. Res., 47, 18, 7019–7026, 2008.
630 Rosas, J. M., Bedia, J., Miraso, J. R., and Cordero, T.: Preparation of hemp-derived
631 activated carbon monoliths, adsorption of water vapor, Ind. Eng. Chem. Res., 47, 4,
632 1288–1296, 2008.
633 Schwarz, J. P., Spackman, J. R., Fahey, D. W., Gao, R. S., Lohmann, U., Stier, P.,
634 Watts, L. A., Thomson, D. S., Lack, D. A., Pfister, L., Mahoney, M. J.,
635 Baumgardner, D., Wilson, J. C., and Reeves, J. M.: Coatings and their enhancement
636 of black carbon light absorption in the tropical atmosphere, J. Geophys. Res., 113,
637 D03203, 2008.
638 Seisel, S., Pashkova, A., Lian, Y., and Zellner, R.: Water uptake on mineral dust and
639 soot: a fundamental view of the hydrophilicity of atmospheric particles, Faraday
640 Discuss., 130, 437–451, 2005.
641 Sjogren, S., Gysel, M., Weingartner, E., Baltensperger, U., Cubison, M. J., Coe, H.,
642 Zardini, A. A., Marcolli, C., Krieger, U. K., and Peter, T.: Hygroscopic growth and
643 water uptake kinetics of two-phase aerosol particles consisting of ammonium
644 sulfate, adipic and humic acid mixtures, Aerosol Science, 38, 157–171, 2007.
645 Song, J., Peng, P., and Huang, W.: Black carbon and kerogen in soils and sediments. 1.
646 Quantification and characterization, Environ, Sci. Technol., 36, 3960–3967, 2002.

https://doi.org/10.5194/acp-2020-110
Preprint. Discussion started: 27 February 2020

Atmospheric Chemistry and Physics Discussions

647 Song, W., and Boily, J. F.: Water vapor adsorption on goethite, Environ. Sci. Technol.,
648 47, 7171–7177, 2013.
649 Stanislav, V., Vassilev, D. B., Andersen, L. K., and Vassileva, C. G.: An overview of
650 the composition and application of biomass ash. Part 1. Phase-mineral and chemical
651 composition and classification, Fuel, 105, 40–76, 2013.
652 Stemmler, K., Vlasenko, A., Guimbaud, C., and Ammann, M.: The effect of fatty acid
653 surfactants on the uptake of nitric acid to deliquesced NaCl aerosol, Atmos. Chem.
654 Phys., 2008, 8 (17), 5127–5141, 2008.
655 Suda, S. R., Petters, M. D., Yeh, G. K. Strollo, C., Matsunaga, A., Faulhaber, A.,
656 Ziemann, P. J., Prenni, A. J., Carrico, C. M., Sullivan, R. C., and Kreidenweis, S.
657 M.: Influence of functional groups on organic aerosol cloud condensation nucleus
658 activity, Environ. Sci. Technol., 48, 10182–10190, 2014.
659 Velasco, L. F., Remy Guillet, N. R., Dobos, G., Thommes, M., and Lodewyckx, P.:
660 Towards a better understanding of water adsorption hysteresis in activated carbons
661 by scanning isotherms, Carbon, 96, 753–758, 2016.
662 Wei, S., Zhu, M., Fan, X., Song, J., Peng, P., Li, K., Jia, W., and Song, H.: Influence
663 of pyrolysis temperature and feedstock on carbon fractions of biochar produced
664 from pyrolysis of rice straw, pine wood, pig manure and sewage sludge,
665 Chemosphere, 218, 624–631, 2019.
666 Xiao, J., Liu, Z., Kim, K., Chen, Y., Yan, J., Li, Z., and Wang, W.: S/O-Functionalities
667 on modified carbon materials governing adsorption of water vapor, J. Phys. Chem.
668 C., 117, 23057−23065, 2013.
669 Xiao, X., Chen, B., Chen, Z., Zhu, L., and Schnoor, J. L.: Insight into multiple and
670 multilevel structures of biochars and their potential environmental applications: A
671 critical review, Environ. Sci. Technol., 52(9), 5027−5047, 2018.

https://doi.org/10.5194/acp-2020-110
Preprint. Discussion started: 27 February 2020

Atmospheric Chemistry and Physics Discussions

672 Yuan, J. F., Huang, X. F., Cao, L. M., Cui, J., Zhu, Q., Huang, C. N., Lan, Z. J., and
673 He, L.Y.: Light absorption of brown carbon aerosol in the PRD region of China,
674 Atmos. Chem. Phys. Discuss., 15, 28453–28482, 2015
675 Yuan, W., Li, X., Pan, Z., Connell, L. D., Li, S., and He, J.: Experimental
676 investigation of interactions between water and a lower silurian chinese shale,
677 Energy Fuels, 28, 4925−4933, 2014.
678 Zhang, R., Khalizov, A., Wang, L., Hu. M., and Xu, W.: Nucleation and growth of
679 nanoparticles in the atmosphere, Chem. Rev., 112, 3, 1957–2011, 2012.
680 Zuend, A., Marcolli, C., Booth, A. M., Lienhard, D. M., Soonsin, V., Krieger, U. K.,
681 Topping, D. O., McFiggans, G., Peter, T., and Seinfeld, J. H.: New and extended
682 parameterization of the thermodynamic model AIOMFAC: Calculation of activity
683 coefficients for organic-inorganic mixtures containing carboxyl, hydroxyl, carbonyl,
684 ether, ester, alkenyl, alkyl, and aromatic functional groups, Atmos. Chem. Phys., 11,
685 9155–9206, 2011.